Full Length Research Paper

2D and 3D geoelectrical resistivity imaging: Theory and field design

Ahzegbobor Philips Aizebeokhai

Department of Physics, Covenant University, Ota, Ogun State, Nigeria. E-mail: Philips_a_aizebeokhai@yahoo.co.uk.

The development of resistivity surveying techniques has been very rapid in the last three decades. The advent of automated data acquisition systems, inversion codes, and easy access to powerful and fast computers has tremendously increased the practical applicability of the geophysical method. Geoelectrical resistivity imaging is increasingly being used in environmental, engineering and hydrological investigations as well as geothermal and mineral prospecting, where detailed knowledge of the subsurface is sought. In this paper, the historical development and basic principles of geoelectrical resistivity surveying techniques are presented. Past researches and on-going developments in the survey designs and field procedures in two-dimensional (2D) and three-dimensional (3D) geoelectrical resistivity surveys are discussed. Current development in the acquisition geometry for 3D geoelectrical resistivity imaging data is emphasized.

Key words: Geoelectrical resistivity, 2D/3D surveys, field design, acquisition geometry, 2D/3D imaging.

INTRODUCTION

Electrical and electromagnetic (EM) methods have been important in the field of Applied Geophysics for about a century, particularly for shallow and near-surface investigations. The use of geoelectrical resistivity surveys for investigating subsurface layered media has its origin in 1912 due to the work of Conrad Schlumberger who conducted the first geoelectrical resistivity experiment in the fields of Normandy; and about 1915, a similar idea was developed by Frank Wenner in the United State of American (USA) (Kunetz, 1966). Ever since, geoelectrical resistivity surveying has greatly improved, and has become an important and useful tool in hydrogeological studies, mineral prospecting and mining, as well as in environmental and engineering applications (e.g. Griffiths et al., 1990; Griffiths and Barker, 1993; Dahlin and Loke, 1998; Olayinka, 1999; Olayinka and Yaramanci, 1999; Amidu and Olayinka, 2006; Aizebeokhai et al., 2010).

The classical methods of geoelectrical resistivity surveys have undergone significant changes in the last three decades. The traditional horizontal layering technique for interpreting geoelectrical resistivity data are rapidly being replaced with two-dimensional (2D) and three-dimensional (3D) models of interpretations, especially in complex and heterogeneous subsurface media. Field techniques have advanced from measure-ments made at separate and independent points to

automated measuring systems with multi-electrode array along the measurement profiles. Data acquisition was more or less carried out manually till the 1980s, and this is labour intensive and slow, and the quality of the measured data might be poor. A range of fast automated multi-electrode and multi-channel data acquisition systems now exist that allows flexibility in the acquisition of geoelectrical resistivity data (Barker, 1981; Stummer and Maurer, 2001; Auken et al., 2006).

Traditionally, electrical resistivity surveying was limited to either delineating the variation of apparent resistivity over a surface or compiling quasi-2D sections from a rather limited numbers of vertical electrical soundings (VES). The use of multi-electrode/multi-channel systems for data acquisition in geoelectrical resistivity surveys has led to a dramatic increase in field productivity as well as increased quality and reliability of subsurface resistivity information obtained. Initially, multi-electrode systems with manual switching (Barker, 1981) were used before the emergence of computer-controlled multi-electrode/multi-channel systems with automatic measurements and data quality control, which has tremendous impact on the quality of the data and the speed with which they are collected. Intelligent multi-electrode with built-in-preamplifiers, analog-to-digital converters, and digital transmission lines can now be

effectively used for data acquisition. Multi-channel transmitter and receiver systems are now being used in simultaneously carrying out series of measurements (Stummer and Maurer, 2001; Auken et al., 2006).

Basic theory of geoelectrical resistivity surveys

Electrical and electromagnetic (EM) methods are defined by their frequency of operation, the origin of the source signals and the manner by which the sources and receivers are coupled to the ground. The signal frequencies range from a few hertz (Hz) in direct-current (DC) resistivity surveys up to several gigahertz (GHz) in ground-penetrating radar (GPR) measurements. The methods are generally governed by Maxwell's equations of electromagnetism (Grant and West, 1965; Ward and Hohmann, 1987). Wave propagation dominates at high frequencies, whereas diffusion is the dominant physical mechanism of electromagnetic induction at lower frequencies (in the quasi-static approximation). In the direct-current (DC) frequency, the diffusion term is zero and the field is thus governed entirely by Poisson equation.

Electrical and electromagnetic methods may either be passive or active. Passive methods use electromagnetic (EM) fields created by natural phenomena as source signals (e.g., telluric currents). In contrast, active methods employ signal generators to generate the required input signals. Sources and receivers can be coupled to the ground through galvanic contacts such as planted electrodes or through EM induction such as coils of wire. These possibilities result in a greater variety of field techniques than any other geophysical surveying method where a single field of force or anomalous property (such as elasticity, magnetism, gravitation or radioactivity) is used.

Electrical methods of geophysical investigations are based on the resistivity (or its inverse, conductivity) contrasts of subsurface materials. The electrical resistance, R of a material is related to its physical dimension, cross-sectional area, A and length, l through the resistivity, ρ or its inverse, conductivity, σ by

$$\rho = \frac{1}{\sigma} = \frac{RA}{l}. \qquad\qquad 1$$

Low-frequency alternating current is employed as source signals in the DC resistivity surveys in determining subsurface resistivity distributions. Thus, the magnetic properties of the materials can be ignored (Telford et al., 1990) so that Maxwell's equations of electromagnetism reduced to:

$$\nabla \cdot \vec{E} = \frac{1}{\varepsilon_0} q \qquad\qquad 2$$

$$\nabla \times \vec{E} = 0 , \qquad\qquad 3$$

where $\vec{E}$ is the electric field in V/m, q is the charge density in C/m^3 and ε_0 is the permittivity of free space ($\varepsilon_0 \cong 8.854 \times 10^{-12} F/m$). These equations are applicable to continuous flow of direct-current; however, they can be used to represent the effects of alternating currents at low frequencies such that the displacement currents and induction effects are negligible.

Usually, a complete homogeneous and isotropic earth medium of uniform resistivity is assumed. For a continuous current flowing in an isotropic and homogeneous medium, the current density $\vec{J}$ is related to the electric field, $\vec{E}$ through Ohm's law:

$$\vec{J} = \sigma\vec{E} . \qquad\qquad 4$$

The electric field vector $\vec{E}$ can be represented as the gradient of the electric scalar potential,

$$\vec{E} = -\nabla\Phi . \qquad\qquad 5$$

By combining Equations 2 and 5, we obtained the fundamental Poisson equation for electrostatic fields given by

$$\nabla^2\Phi(x, y, z) = -\frac{1}{\varepsilon_0} q(x, y, z) . \qquad\qquad 6$$

The equation of continuity for a point in 3D space and time t defined by the Dirac delta function is given as:

$$\nabla \cdot \vec{J}(x, y, z, t) = -\frac{\partial}{\partial t} q(x, y, z, t)\delta(x)\delta(y)\delta(z) . \qquad 7$$

The current sources in a typical electrical resistivity survey are usually point sources. Thus, the current and the current density over a volume element, ΔV around a current source, I located at (x_s, y_s, z_s) are given by the relation (Dey and Morrison, 1979) as:

$$\nabla \cdot J = \left(\frac{I}{\Delta V}\right)\delta(x - x_s)\delta(y - y_s)\delta(z - z_s), \qquad 8$$

where δ is the Dirac delta function. Hence, the potential distribution in the ground due to a point current source is

$$-\nabla \cdot [\sigma(x, y, z)\nabla\Phi(x, y, z)] = \left(\frac{I}{\Delta V}\right)\delta(x - x_s)\delta(y - y_s)\delta(z - z_s)$$

.   9

This partial differential equation, which is a self-adjoint, strongly connected and non-separable elliptic equation of second order, gives the subsurface potential distribution in an isotropic non-uniform 3D medium due to a point current source. Numerous techniques have been developed to solve this problem, that is, to determine the potential distribution that would be observed over a given subsurface structure. The potential, $\Phi(x, y, z)$ and the normal component of the current density, $\sigma\frac{\partial\Phi}{\partial n}$ are continuous across the boundary between two media of different resistivities but the current lines are refracted in accordance to the boundary conditions.

Potential distribution due to point source in a homogeneous half-space

All resistivity methods employ an artificial source of current injected into the subsurface through point electrodes and the resulting potential difference is measured at other electrodes positions in the neighbourhood of the current flow. For a semi-infinite conducting layer of uniform resistivity (a completely homogeneous and isotropic medium) bounded by the ground surface as shown in Figure 1, a current of strength +I is injected at a point C_1 into the ground surface. This current will flow away radially from the point of entering and its distribution will be uniform over a hemispherical shell of an underground region (Figure 2) of resistivity ρ. At a distance r of a point in the medium from the point source, the surface area of the hemispherical shell is $2\pi r^2$ so that the potential for the homogeneous half-space is

$$\Phi(r) = \frac{\rho I}{2\pi r}.$$ 10

In practice, two current electrodes, the current source +I and the sink –I (Figure 1), are usually used. The potential distribution is symmetrical about the vertical placed at the mid-point between the two current electrodes. The potential at an arbitrary point from a given pair of current electrodes, by applying Equation 10, is obtained as

$$\Phi(r) = \frac{\rho I}{2\pi}\left(\frac{1}{r_{C1}} - \frac{1}{r_{C2}}\right),$$ 11

where r_{C1} and r_{C2} are the respective distances from the

first (source) and second (sink) current electrodes to the arbitrary point.

Apparent resistivity and geometric factor

Usually, it is the potential difference between two points that is measured. The injecting (current) electrodes could be used, in theory, to measure the potential difference. But the influence of the resistances between the subsurface and current electrodes is not precisely known (Cheng et al., 1990). Thus, two potential electrodes are dedicated to detect the response signal. If P_1 and P_2 are the potential electrodes (Figure 1), the potential difference between P_1 and P_2 becomes

$$\Delta\Phi = \frac{I\rho}{2\pi}\left(\frac{1}{C_1P_1} - \frac{1}{C_1P_2} - \frac{1}{C_2P_1} + \frac{1}{C_2P_2}\right).$$ 12

This equation gives the potential that would be observed over a homogeneous half-space with a typical four electrodes configuration. The subsurface is typically heterogeneous so that the resistivity observed is apparent, that is, the resistivity of a homogeneous subsurface medium that would give the same resistivity value for the same electrode configuration. Apparent resistivity can be seen as a weighted average of the resistivities of the subsurface volume under the four electrodes. The apparent resistivity depends on the configuration of the electrodes and is determined by the injected current I and voltage $\Delta\Phi$. Thus, the apparent resistivity ρ_a is expressed as

$$\rho_a = G\frac{\Delta\Phi}{I}.$$ 13

The geometric factor G in the above expression, which depends on the electrode configuration, is given as

$$G = 2\pi / \left(\frac{1}{C_1P_1} - \frac{1}{C_1P_2} - \frac{1}{C_2P_1} + \frac{1}{C_2P_2}\right).$$ 14

Field design and survey procedure

Near-surface sources usually treated as noise in traditional geophysical exploration surveys are often the targets of interest in hydrological, environmental and engineering investigations. The subsurface geology is usually complex, subtle and multi-scale such that spatial variations can change rapidly both laterally along the survey profiles and vertically with depths. Thus, a closely spaced grid of observation points is required for the accurate characterization, high spatial resolution and
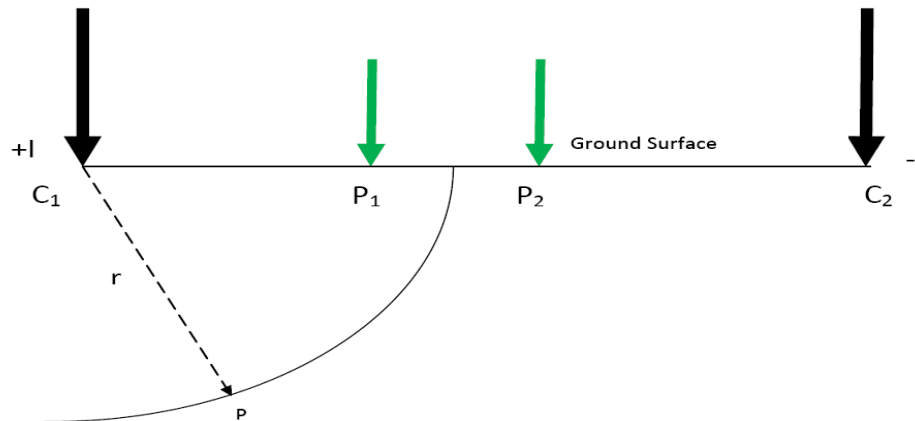
Figure 1. Potential distribution due to a current source in a homogeneous half-space.
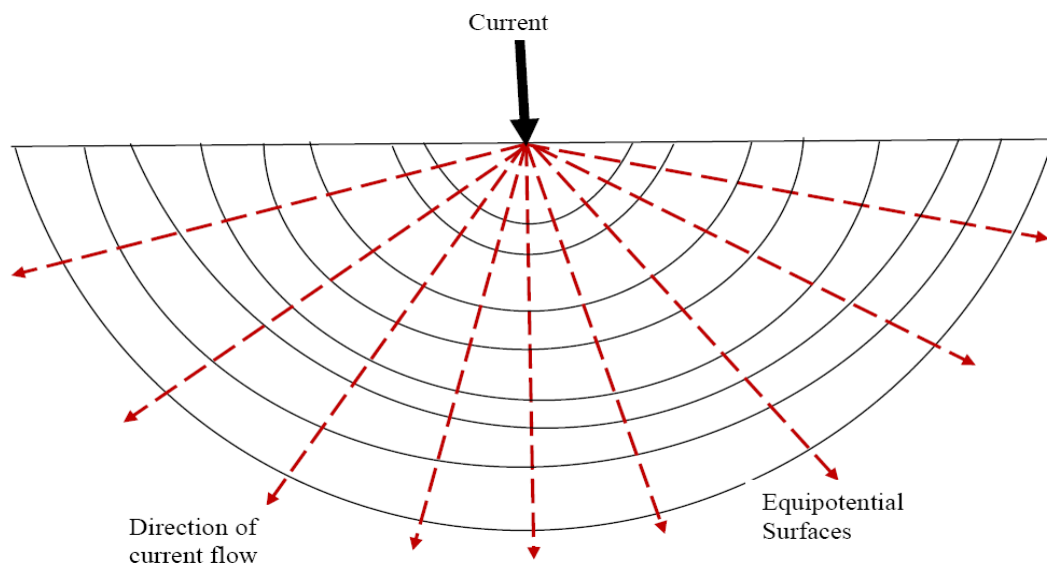

Figure 2. Current from a point source and the resulting equipotential distributions.

good target definition of such highly heterogeneous subsurface. Survey design must take into account the capabilities of the data acquisition system, heterogeneity of the subsurface electrical conductivity and the required resolution. Other factors to be considered are the areal extent of the site to be investigated, the cost of the survey and the time required to complete the survey.

Electrode configurations

Four electrodes are generally placed at arbitrary locations (Figure 1); however, a number of electrode configurations have been used in recording resistivity field data, each suitable for a particular geological situation. The conventional arrays most commonly used include Wenner (alpha), Schlumberger, dipole-dipole, pole-pole

and pole-dipole arrays. These arrays with their corresponding geometric factor are illustrated in Figure 3. The apparent resistivity values observed by the different array types over the same structure can be very different. The choice of a particular array depends on a number of factors, which include the geological structures to be delineated, heterogeneities of the subsurface, sensitivity of the resistivity meter, the background noise level and electromagnetic coupling. Other factors to be considered are the sensitivity of the array to vertical and lateral variations in the resistivity of the subsurface, its depth of investigation, and the horizontal data coverage and signal strength of the array.

The conventional Wenner (alpha) and Schlumberger arrays are relatively sensitive to vertical variations in the subsurface resistivity below the centre of the array but less sensitive to horizontal variations in the subsurface
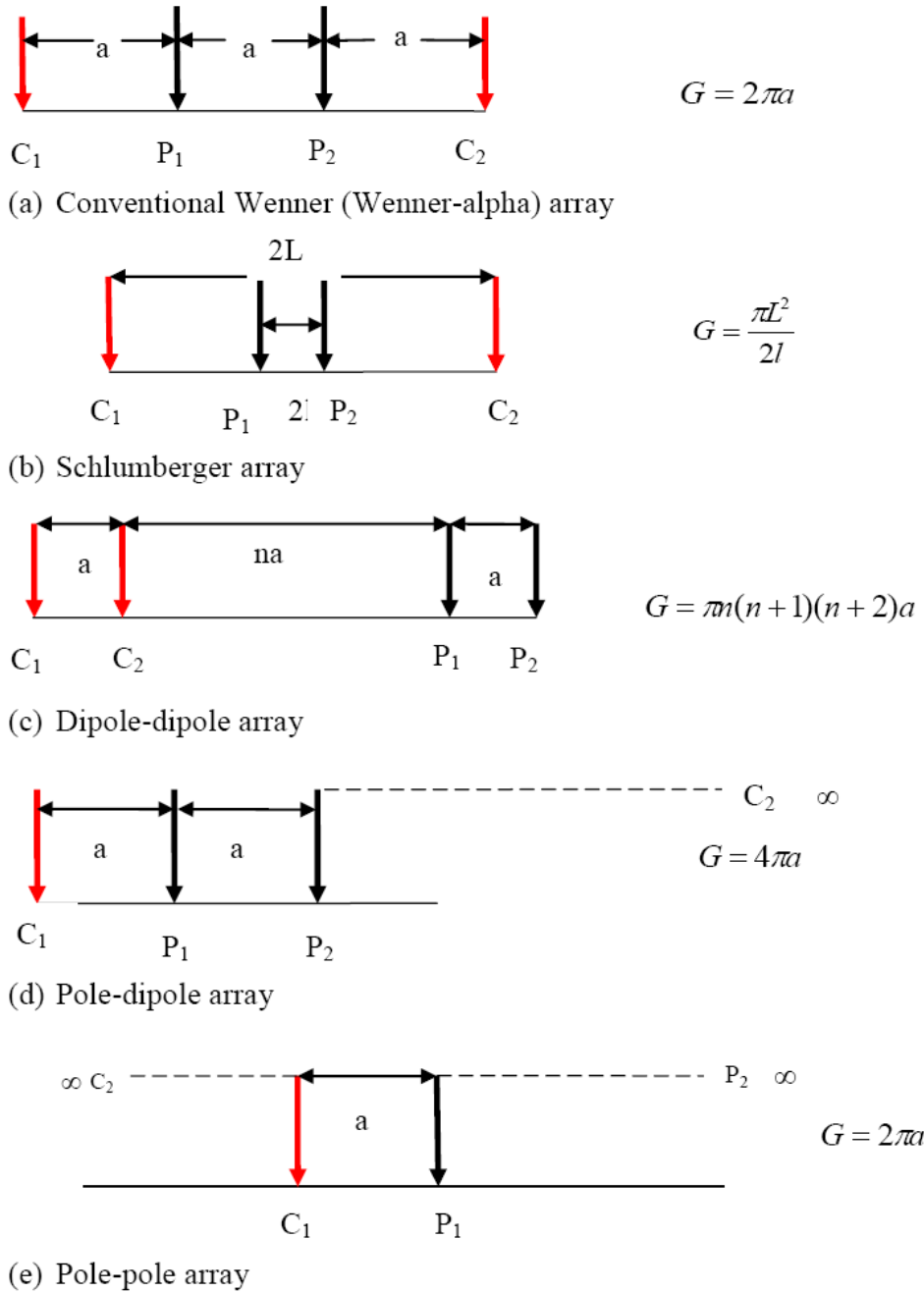
$$G = 2\pi a$$

(a) Conventional Wenner (Wenner-alpha) array

$$G = \frac{\pi L^2}{2l}$$

(b) Schlumberger array

$$G = \pi n(n+1)(n+2)a$$

(c) Dipole-dipole array

$$G = 4\pi a$$

(d) Pole-dipole array

$$G = 2\pi a$$

(e) Pole-pole array

Figure 3. Conventional electrode configurations commonly used in geoelectrical resistivity surveys with their corresponding geometric factors.

resistivity. The arrays have moderate depths of investigation and generally strong signal strength which is inversely proportional to the geometric factor used in calculating the apparent resistivity values. The major limitation of these arrays is the relatively poor horizontal coverage with increased electrode spacing. Wenner array is preferred for surveys in a noisy site because of its high signal strength; however, the array is less sensitive to 3D structures (Dahlin and Loke, 1997).

The dipole-dipole array is the most sensitive to resistivity variations below the electrodes in each dipole pair and is very sensitive to horizontal variations but relatively insensitive to vertical variations in the subsurface resistivities. Thus, it is the most preferred array for mapping vertical structures like dykes and cavities. Dipole-dipole array is, however, very poor in mapping horizontal structures such as sills, sedimentary or horizontal layers. In addition, it is the most sensitive

array to 3D structure among the common arrays (Dahlin and Loke, 1997). The depth of investigation of the array depends on both the current electrode spacing, a and the distance between the two dipoles; and is generally shallower than that of Wenner array. However, dipole-dipole array has better horizontal data coverage than Wenner array. The major disadvantage of this array is the decrease in signal strength with increasing distance between the dipole pair.

The pole-dipole array is an asymmetrical array with asymmetrical apparent resistivity anomalies in the pseudosections over a symmetrical structure, which could influence the inversion model. It has relatively good horizontal coverage and higher signal strength compared with dipole-dipole array. It is much less sensitive to telluric noise than the pole-pole array. Repeating measurements with the electrodes arranged in the reverse order can eliminate the asymmetrical effect. The combined measurements of the forward and reverse pole-dipole array would remove any bias in the model due to asymmetry. However, this will increase the survey time as the number of data points to be measured will be doubled. The signal strength of the pole-dipole array is lower than that of Wenner and Schlumberger arrays, and is very sensitive to vertical structures.

The pole-pole array consists of one current and one potential electrode with the second current and potential electrodes at infinite distances. Finding suitable locations for these electrodes so as to satisfy this theoretical requirement is often difficult. In addition to this limitation, the pole-pole array is highly susceptible to large amount of telluric noise capable of degrading the quality of the observed data. However, the pole-pole array has the widest horizontal coverage and the deepest depth of investigation but the poorest resolution. The resolution of the pole-pole array is very poor as subsurface structures tend to be smeared out in the inversion model (Dahlin and Loke, 1997). If the electrode spacing is small and good horizontal coverage is desired, the pole-pole array is a reasonable choice.

Apart from these conventional arrays, many non-conventional electrode configurations have been studied (Stummer et al., 2004; Wilkinson et al., 2006). For n equally spaced collinear electrodes, there exist a number of non-reciprocal four-point electrode configurations (Noel and Xu, 1991) given by:

$$n_d = \frac{1}{8} n(n-1)(n-2)(n-3). \qquad 15$$

These measurements set include every possible conventional and non–conventional electrode arrays. Measurements with this set of electrode configurations results in comprehensive data sets which would contain all resistivity subsurface information that the n-electrodes system is capable of gathering. However, a large portion of these configurations have large geometric factors

capable of reducing the stability of the inversion of the observed data sets. Stummer et al. (2004) assessed the imaging potential of the data sets acquired with modern multi-electrode resistivity systems using synthetic and field examples. They showed that comprehensive data sets recorded with large numbers of four-point electrode configurations provides significantly more information than those with standard electrode arrays. However, the recording of comprehensive data sets requires too many measurements and is therefore not cost effective in routine geoelectrical resistivity surveys.

An optimization procedure that utilizes a goodness function that ranks the sensitivities of all electrode configurations can be used to define suite of electrode configurations that yields images comparable in quality to those obtained from comprehensive data sets (Wilkinson et al., 2006; Furman et al., 2007; Hennig et al., 2008). The goodness function includes weighting terms which counterbalance the high sensitivities of the model relative to deeper parts and minimize the influence of well resolved regions of the model based on the experimental design procedure. Measurements are initially made on coarse arrays, with subsequent electrode configurations optimised according to the result of previous measurements. Data generated with electrode configurations that yields large amounts of new information according to their high sensitivities and depth of influence are incorporated into the successively increasing optimal data sets. Fast online inversion schemes are required to update the model estimates between measurements and to find the optimal array configurations (Maurer et al., 2000; Stummer et al., 2004; Auken et al., 2006).

Data acquisition instruments

Geoelectrical resistivity field data are acquired using earth resistivity meter commonly referred to as Terrameter. The equipment is portable, light weight and relatively cost effective when compared with other geophysical data acquisition systems. A conventional set-up of the earth resistivity meter (Figure 4) basically consists of the following: a constant current source, commonly a battery pack connected to a commutated DC circuit to change polarity of the current source; an ammeter which measures the injecting current; a very sensitive voltmeter that measures the response signal; four metal stake electrodes, usually stainless steel or non-polarizing $Cu - CuSO_4$ and $Ag - AgCl_2$, which ensures low impedance characteristic; and four cable reels used in connecting the electrodes to the current source and voltmeter. A low frequency AC signal may be used as current source instead of a commutated DC source (Christensen, 1989). The internal impedance of the ammeter, connected in series with the current source, should be low so as to minimize its effect on the
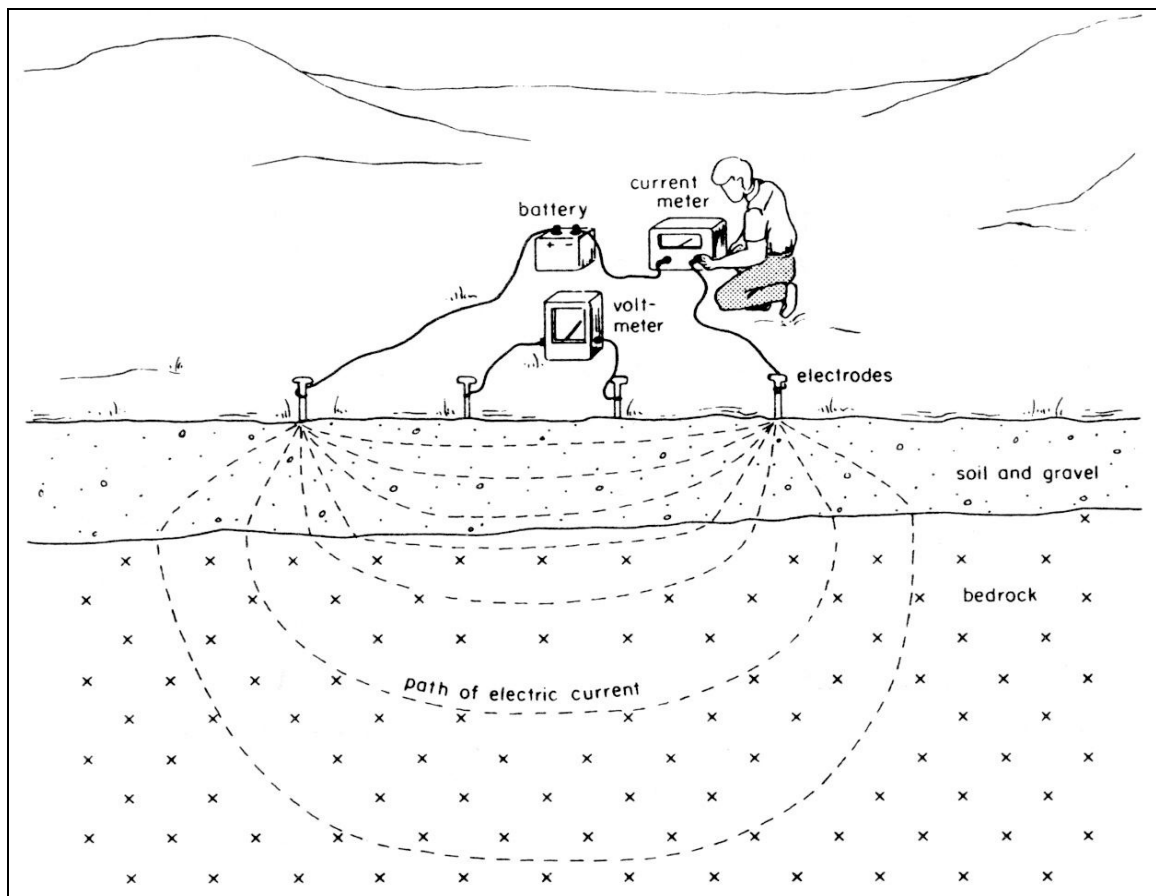
Figure 4. A conventional set-up of the earth resistivity meter geoelectrical resistivity field observations (after Robinson and Coruh, 1988).

measuring circuit. Similarly, the voltmeter connected in parallel with the ammeter should have high input impedance so as to suppress any effect arising from the ammeter. In general, the current source and both meters are usually housed in a single box.

Acquiring field data using the set-up shown in Figure 4 is usually time consuming and labour intensive, as it involve the movement of the four electrodes from one point to another for each data point to be measured. A minimum of one person is required to handle each of the electrodes with its connecting cable and an additional person is needed to handle the recording equipment, thus making a minimum of five-man data collection crew in a typical survey. The development of multi-electrode data acquisition systems has greatly improved the speed and reduced the cost of acquiring field data. With multi-electrode systems, two or three persons can conveniently carry out field surveys especially in 2D and 3D resistivity imaging where large volumes of data are required. The automated multi-electrode systems offer efficient means of acquiring field data in arbitrary four-point electrode configurations, thus allowing flexibility in the choice of electrode configuration(s) in a given survey.

The automated systems generally consist of a resistivity instrument, a relay unit (electrode selector), a portable computer, electrode cables, various connectors and electrodes (e.g. Griffiths et al., 1990). Two or more components of the multi-electrode systems may be housed in the same box, making the systems more compact and portable. Some multi-electrode systems employ intelligent switches with built-in-amplifiers (Stummer and Maurer, 2001; Stummer et al., 2004) at each electrode take-out instead of a central switching unit. Other features of the multi-electrode systems that enhanced productivity and quality of data acquired are analog-to-digital converters and digital transmission lines. The automated multi-electrode systems are either single channel or multi-channel. The multi-channel systems consist of multi-channel transmitters and receivers that enable them to simultaneously carry out series of measurements. For any N-channel multi-electrode systems, N numbers of data can be recorded simultaneously thereby increasing the data acquisition speed by a factor of N. A number of multi-electrode systems are commercially available for shallow investigations, such as the Geo Tom (Geolog), Tomoplex
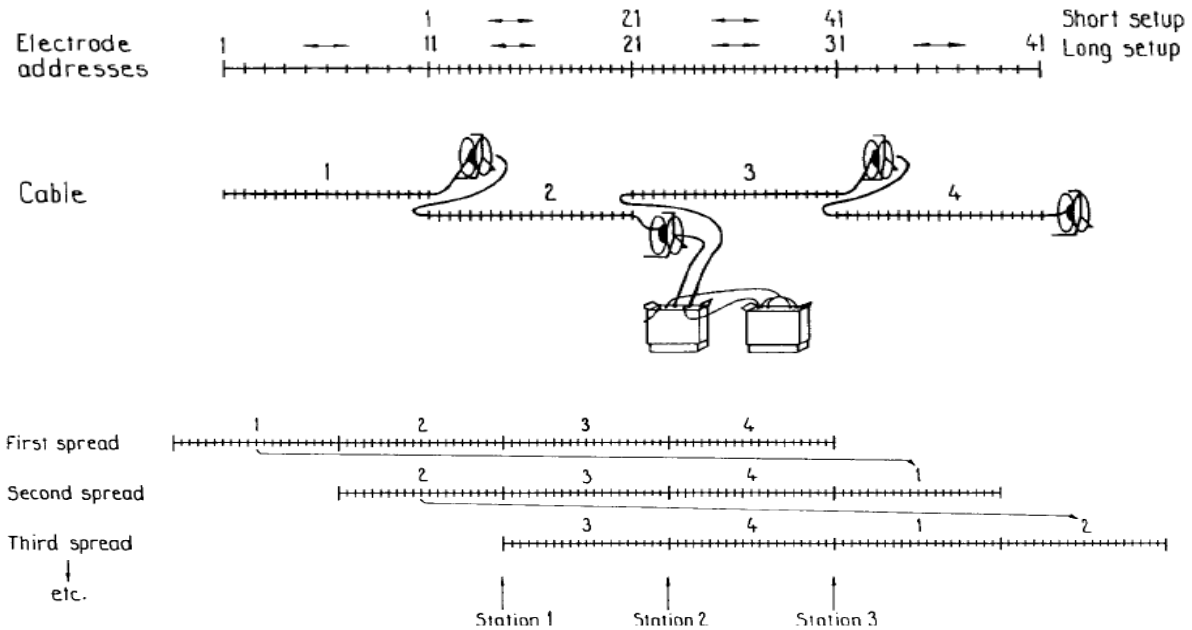
Figure 5. Schematic layout of automatic data acquisition system using four electrode cables, indicating the roll-along technique (after, Overmeeren and Ritsema, 1988).

(Campus Ltd), Super String R8 (AGI Inc), SAS 4000 Lund (ABEM) and RESECS (DTM GmbH).

In field surveys, the cables are rolled out along the survey line(s) as pre-designed by the field crew and the electrodes are connected to the electrode take-outs which are usually numbered on the cables. Two to four cables may be used together in a given survey depending on the acquisition system and the electrode configuration used. The electrode take-out number should increase in the direction of increasing coordinate number. The acquisition systems automatically check the electrode contacts and scan through a pre-defined measurement protocol. The extension of the survey line can be achieved through roll-along technique (Figure 5) in which part of the layout is shifted along the survey line so as to make new measurements in areas not already covered. The systems allow automatic updating of the coordinates in both x- and y-axes when roll-along along technique is adopted.

The development of microprocessors in data acquisition instruments and continuous measurement systems has significantly enhanced the usefulness of geoelectrical resistivity imaging. Large and dense measurements can now be made efficiently and economically over wide areas without sacrificing lateral resolution (Auken et al., 2006). The continuous measurement systems have fixed-electrode configurations capable of making measurement continuously while moving on the ground; this has greatly increased data acquisition speed in 2D/3D geoelectrical resistivity imaging. Common examples of the continuous

measurement systems include the PACES system (Sorensen, 1996), multiple continuous electrical profiling (MUCEP) system (Panissod et al., 1998) and Geometrics' OhmMapper system (Pellerin, 2003). The PACES system uses galvanically coupled steel-cylinder electrodes mounted on a tail. The MUCEP system uses spiked wheels as electrodes or capacitively coupled electrodes mounted inside plastic wheels; and the Geometric OhmMapper system uses capacitively coupled line electrodes.

Developments in geoelectrical resistivity methods have enhanced the ability of resistivity imaging in under-water (marine or fresh water) environments to reproducing the resistivity structure of the sediments beneath the water (e.g. Breier et al., 2005; Kwon et al., 2005; Day-Lewis et al., 2006; Amidu and Dunbar, 2007; Mansoor and Slater, 2007). Continuous resistivity profiling (CRP) in which multi-electrode are mounted on streamers towed behind a boat is commonly used in under-water environments. The streamers can be dragged along the water bottom or float on the surface of the water to avoid any under-water obstacle. Floating the electrodes on the surface of the water is most useful in relatively shallow areas. Usually, two of the electrodes are used as current electrodes and all other as potential electrodes. The streamers are usually coupled with a bathymetry profiler and a water conductivity meter. Major applications of under-water resistivity survey include mapping zones of submarine groundwater discharge into coastal environments, groundwater-surface water interaction studies, and delineation of fresh water zones in coastal aquifers.
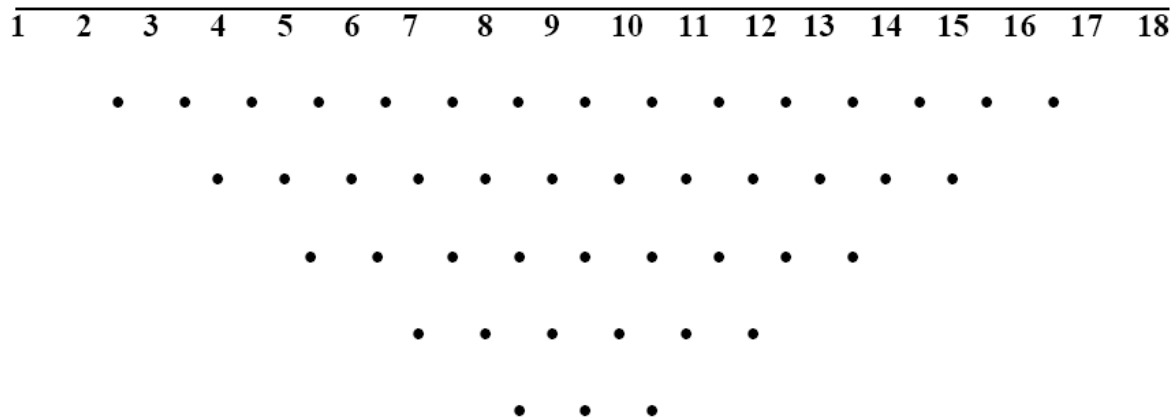
Figure 6. Pseudosection for 5-data levels obtained for Wenner surveys with 18 electrodes (1, 2, 3, ..., being electrode positions).

Salinity studies of lakes and water reservoirs.

Two-dimensional (2D) and three-dimensional (3D) Geoelectrical resistivity surveying

Two-dimensional (2D) geoelectrical resistivity imaging can be achieved by integrating the techniques of vertical electrical sounding with that of electrical profiling. It involves apparent resistivity measurements from electrodes placed along a line using a range of different electrode separations and midpoints. The procedure is repeated for as many combinations of current and potential electrode positions as defined by the survey configuration. 2D resistivity imaging can be seen as continuous vertical electrical sounding (CVES) in which a number of VES conducted in a grid are merged together or as a combination of successive profiles with increasing electrode spacing.

Two-dimensional (2D) resistivity surveys are usually carried out using large numbers of electrodes connected to multi-core cables. For a system with limited number of electrodes, the area covered by the survey can be extended along the survey line using the roll-along technique (Dahlin and Bernstone, 1997). This can be achieved by moving the cables past one end of the line by several units of electrode spacing, after completing a sequence of measurements (Figure 5). A number of arrays have been used in recording 2D geoelectrical resistivity field data, each suitable for a particular geological situation. The conventional arrays most commonly used include Wenner, dipole-dipole, pole-pole and pole-dipole. Most of the pioneering works in 2D geoelectrical resistivity surveys were carried out using Wenner array (e.g. Griffiths and Turnbull, 1985; Griffiths et al., 1990; Oldenburg and Li, 1999; Olayinka and Yaramanci, 2000).

The resistivity of the 2D model is assumed to vary both vertically and laterally along the survey line but constant

in the direction perpendicular to the survey line. The observed apparent resistivity values are commonly presented in pictorial form using pseudosection contouring (Figure 6) which gives an approximate picture of the subsurface resistivity distribution. The shape of the contours depends on the type of array used in the investigation as well as the distribution of the true subsurface resistivity. The pseudosection plot serves as a useful guide for detail quantitative interpretation. Poor apparent resistivity measurements can easily be identified from the pseudosection plot. The pseudo-depth values are based on the sensitivity values or the Frechet derivatives for a homogenous half-space.

All geological structures and spatial distribution of subsurface petrophysical properties are inherently three-dimensional in nature. The three-dimensional effects of subsurface structures are more pronounced in environmental and engineering investigations where the geology is highly heterogeneous and subtle. Model images resulting from 2D resistivity surveys often contain spurious features due to 3D effects and violation of the 2D assumption. This usually leads to misinterpretation of the observed anomalies in terms of magnitude and location (Bentley and Gharibi, 2004). Hence, a 3D survey with a 3D interpretation model in which the resistivity is allowed to vary in all directions should, in theory, give the most accurate and reliable results especially in subtle heterogeneous subsurface.

What constitute a 3D data set that would yield significant 3D subsurface information for geoelectrical resistivity imaging is not clearly understood. Ideally, the measurements of apparent resistivity values that would constitute a complete 3D data set should be made in all possible directions. The techniques for conducting 3D electrical resistivity surveys have been presented by Loke and Barker (1996). The use of pole-pole (Li and Oldenburg, 1994; Loke and Barker, 1996; Park, 1998) and pole-dipole (Chambers et al., 1999; Ogilvy et al., 1999) arrays in 3D electrical resistivity surveys have been
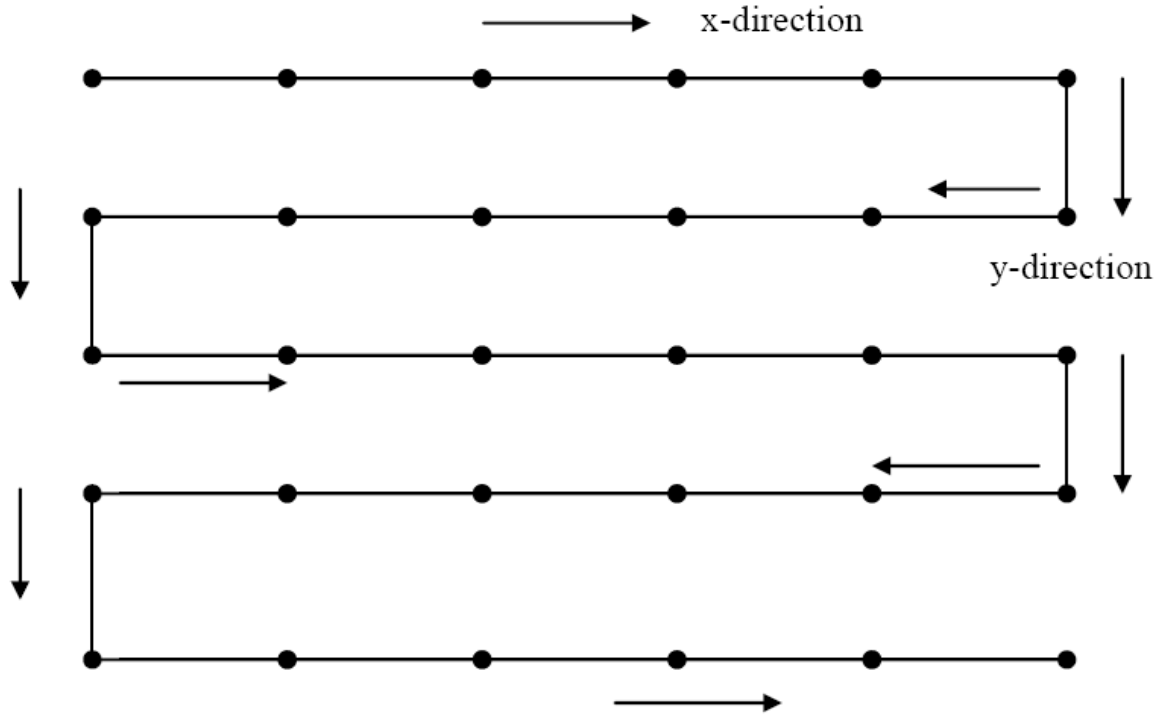
Figure 7. The arrangement of electrodes for a 6 by 5 grid in a 3D resistivity survey.
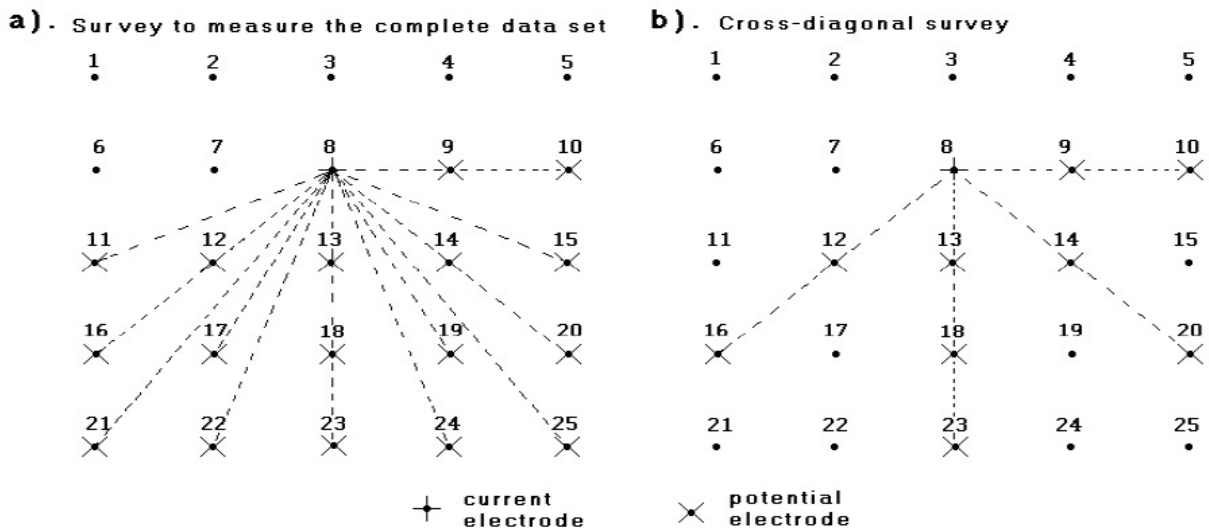

Figure 8. Two possible measurement sequences for a 3D geoelectrical resistivity survey with potential electrodes corresponding to a single current electrode in (a) a complete data set survey and (b) cross-diagonal survey (after Loke and Barker, 1996).

reported. Square and rectangular grids of electrodes with constant electrode spacing in both x- and y-directions (Figure 7), in which each electrode is in turn used as current electrode and the potential measured at all other electrode positions (Figure 8a), were commonly used. For n number of electrodes in a grid, the maximum number of independent data points (a complete 3D data set) that can be measured (Xu and Noel, 1993) is given by:

$$d_{max} = \frac{n(n-1)}{2}.$$

16

For a 10 by 10 grid (100 electrodes), for example, a 3D survey with a complete data set would yield 4500 data points. Such a complete data set measurement is time consuming and impractical in large surveys involving large number of electrodes in the grid.

But these methods are usually impractical because of the length of cables, the number of electrodes, the site geometry and electrode spacing involved in practical surveys. In addition, the measurements 3D data sets using the square or rectangular grids of electrodes is time consuming and cumbersome in surveys involving large grids since the number of possible electrode permutations for the measurements will be very large. To reduce the number of measurements and the time required to carry out a 3D resistivity survey, Loke and Barker (1996) proposed a cross-diagonal survey method in which potential measurements are only made at the electrodes along the x-axis, y-axis and 45-degrees diagonal lines passing through the current electrodes (Figure 8b).

The cross-diagonal surveying method still involves very large number of independent measurements of apparent resistivity data for medium to large grids of electrodes. Thus, acquiring 3D data using cross-diagonal technique would also be time consuming, especially if a single channel or a manual data acquisition system is employed. The inversion of these large volumes of data is often problematic because the computer memory may not be sufficient for the memory space required for the inversion, and stability and convergence in the inversion is often difficult to attain. Most practical/large scale 3D resistivity surveys involve grids of 16×16 electrodes or more to cover a reasonable area. This will require a minimum of 256 electrodes (for 16×16 grids), which is far more than that available on many multi-electrode resistivity meter systems. The roll-along technique used in 2D surveys can be extended to 3D surveys (Dahlin and Bernstone, 1997) to get around this limitation; however, it is also cumbersome.

Apart from these limitations in 3D field measurements, the pole-pole array that has been commonly used is highly susceptible to telluric noise which can significantly degrade the quality of the observed data. Subsurface features tend to smear out in the inversion model obtained because of the poor resolution of pole-pole array. The array requires that two electrodes, one current and one potential, be place at infinite distances from the survey site; getting a suitable position to satisfy this theoretical requirement is often difficult and sometimes impossible in most practical surveys. The effect of these electrodes at infinity on the measured data can be significant, thus making it difficult for the field measurements to meet condition of reciprocity (Park and Van, 1991).

Pole-dipole array has been an attractive alternative to pole-pole array in 3D resistivity surveys (Chambers et al., 1999; Ogilvy et al., 1999) involving medium to large grids

(12 by 12 and above). It offers better resolution than pole-pole array (Sasaki, 1992; 1989) and is less susceptible to telluric noise since both potential electrodes are within the survey grid. However, pole-dipole is an asymmetrical array because of the second current electrode placed at infinity. Measurements can be made in the forward and reverse directions to remove asymmetrical effects on the inversion model. This would increase the time required for the survey as the data points would be doubled.

In contrasts to the cross-diagonal surveying method, sets of parallel 2D lines (Chambers et al., 2002; Bentley and Gharibi, 2004) and orthogonal 2D lines (Aizebeokhai et al., 2009; 2010) which allow flexible survey design, choice of array and easy adaptability to data acquisition systems have been used to construct 3D images. The major challenge of using the parallel or orthogonal 2D profile methods is the optimum inter-line spacing relative to the minimum electrode separation. Ideally, the inter-line spacing should be the same with the minimum electrode separation so as to obtain good quality and high resolution images. For practical purposes, inter-line spacing up to four times the minimum electrode separation would yield good quality inverse models with acceptable resolution. Larger interline spacing will produce more near-surface artefacts in the inversion images.

The resolution of model parameters is significantly improved when the observed data are less noisy. Ambient signal noise, spatial configuration errors, instrument malfunction, ill-determined and poorly under-stood recording parameters, and phenomena associated with the measuring process are major contributors to data errors and noise in the measurements. Limited spatial distribution of electrodes in the arrays and discrete spatial sampling usually result in an insufficient data set. More measurements are often made and stacked to enhance accuracy of each data point. The development of high speed microprocessor in data acquisition systems has made real-time noise-reduction procedures possible. The availability of all measured data makes it possible to specify and quantify the statistical properties of the noise, and explicitly to formulate a noise model, which is extremely important for optimal and meaningful inversion of the resulting data set (Auken et al., 2006).

The resolution of surface geoelectrical resistivity surveys generally decreases with depth and very long layouts are needed to archive large depth penetrations. The presence of a conductive layer at the surface can significantly reduce the depth of penetration. The existing surface configurations or computer modelling techniques have not been able to overcome this fundamental physical limitation. Borehole resistivity imaging, often referred to as electrical resistivity tomography (ERT), can be used to overcome the problem of depth limitation to obtain higher resolution at depths since the electrodes are closer to the structures of interest. The strong influence of near-surface inhomogeneities on inversion

results will also be reduced. 2D and 3D model images that reflect the true subsurface resistivity contrast can be obtained from borehole resistivity tomography (La Breque et al., 1996; Ramirez et al., 1996; Brown and Slater, 1999).

The measurements may be done by arranging the electrodes in the borehole(s) only or borehole and surface so that we can have the following combinations: borehole-to-borehole (or multiple boreholes) measurements (Daily and Owen, 1991; Shima, 1992; Spies and Ellis, 1995; Bing and Greenhalgh, 2000; Slater et al., 2000); borehole-to-surface measurements (Becv and Morrison, 1991; Dhu and Heinson, 2004); and borehole-to-borehole-to-surface measurements (Binley et al., 2002). In general, any array used for surface resistivity survey can be adapted for borehole resistivity measurements; but pole-pole (Daily and Owen, 1991; Shima, 1992; Spies and Ellis, 1995), pole-dipole (Bing and Greenhalgh, 1997; Zhou and Greenhalgh, 2000) and dipole-dipole (Sasaki, 1992; Zhou et al., 2002) arrays are commonly used in borehole resistivity surveys. Based on sensitivity pattern and anomaly effect, the pole-dipole and dipole-dipole arrays have been shown to have better target definition and delineation properties than the pole-pole array.

Geoelectrical resistivity imaging in which the spatial and temporal variations of subsurface resistivity are studied is referred to as time-lapse resistivity imaging or resistivity monitoring. Time series of 2D or 3D images of resistivity distribution are usually collected. Time-lapse resistivity imaging is used in monitoring systems for flow and solute transport in unsaturated zone (Newmark et al., 1998; Slater et al., 2002; Cassian et al., 2006); understanding spatial distribution and temporal behaviour of near surface hydrological processes (Bethold et al., 2004; Rein et al., 2004); and monitoring and delineating groundwater pollution, saline water intrusion, chemical flux and leakage from contaminant structures (Bently and Garibi, 2004; Leroux and Dahlin, 2006).

Time-lapse resistivity surveys may be categorized into permanent, semi-permanent and mobile systems depending on the degree of installation (Aaltonen, 2001). In permanent systems, the electrodes and the cables are permanently installed on the survey sites. This allows for flexible data acquisition with time, though it is expensive because of the construction work needed for the installation. Data and images obtained from these systems are more accurate than other resistivity monitoring systems. The electrodes in semi-permanent systems are permanently installed but the cables and instruments are mobile. Semi-permanent systems are less flexible for data acquisition but less complicated and cheaper than the permanent systems. Mobile systems, on the other hand, practically involve the repetition of resistivity imaging at the same locations. No installations are needed but the data and images are less accurate as electrode positions may not be precise between the time

steps.

Usually, independent inversions of the data set observed at different times are carried out. Smoothness-constrained least-squares inversion method (de Groot-Hedlin and Constable, 1990) is frequently used. This allows the changes in subsurface resistivity values to be determined by comparing the model resistivity values obtained from the inversion of the initial data set with that of a later data set. However, joint inversion technique in which the model obtained from the inversion of the first data set is used as a reference model to constrain the inversion of later time-lapse data set can yield better results (Loke, 1999).

Conclusions

The use of automated multi-electrode data acquisition systems has made 2D and 3D geoelectrical resistivity imaging increasingly being applied to hydrological, environmental and geotechnical investigations. Model images resulting from 2D resistivity surveys often contain spurious features due to 3D effects and violation of the 2D assumption. Since subsurface features are inherently three-dimensional, a 3D survey with a 3D interpretation model should give the most accurate and reliable results especially in subtle heterogeneous subsurface.Square and rectangular grids of electrodes with constant electrode spacing in x-y plane or directions commonly used for 3D surveys yield large volume of independent data points that might be difficult to invert. Cross-diagonal survey method in which potential measurements are made at the electrodes along the x-axis, y-axis and 45-degrees diagonal lines passing through the current electrodes can reduce the number of measurements and the time required to carry out a 3D resistivity survey.

The use of orthogonal or parallel set of 2D profiles for 3D surveys, with inter-line spacing in the order of four times the minimum electrode separation, would made 3D survey much easier and less expensive, and offers much flexibility in the choice of electrode arrays. 2D and 3D model images that reflect the true subsurface resistivity contrast can be obtained from borehole surveys (electrical resistivity tomography) with the strong influence of near-surface inhomogeneities on inversion results being considerably reduced. Arrays used for surface resistivity surveys can be adapted for borehole resistivity measurements; however, pole-dipole and dipole-dipole arrays have been shown to have better target definition and delineation properties.

The resolution of model parameters is significantly improved when the data are less noisy. The accuracy of each data point can be enhanced by making more measurements and stacking them together. The development of high speed microprocessor in data acquisition systems has made real-time noise-reduction procedures possible. The statistical properties of the

noise can now be quantified and specified. This is used for formulating noise model which is useful for optimal and meaningful inversion of the resulting data set.

REFERENCES

Aaltonen J (2001). Seasonal resistivity variations in some different Swedish soils. Eu..J. Environ. Eng. Geophys., 6: 33-45.

Aizebeokhai AP, Olayinka AI, Singh VS (2009). Numerical evaluation of 3D geoelectrical resistivity imaging for environmental and engineering investigations using orthogonal 2D profiles, SEG Expanded Abstracts 28, 1440: 1440-1444, DOI: 10.1190/1.3255120.

Aizebeokhai AP, Olayinka AI, Singh VS (2010). Application of 2D and 3D geoelectrical resistivity imaging for engineering site investigation in a crystalline basement terrain, southwestern Nigeria. Journ. Environ. Earth Scien., DOI: 10.1007/s12665-010-0474-z, p. 1481.

Amidu SA, Dunbar JA (2007). Integrating continous resistivity profiling (CRP) into water reservoir salinity studies – numerical and field evaluation. SEG Expanded Abstracts, 26: 1172-1176.

Amidu SA, Olayinka AI (2006). Environmental assessment of sewage disposal systems using 2D electrical resistivity imaging and geochemical analysis: A case study from Ibadan, Southwestern Nigeria. Environ. Eng. Geosci., 7(3): 261-272.

Auken E, Pellerin L, Christensen NB, Sorensen K (2006). A survey of current trends in near-surface electrical and electromagnetic methods. Geophys., 71(5): 249-260.

Barker RD (1981). The offset system of electrical resistivity sounding and its use with multicore cable. Geophy. Prosp., 29: 128-143.

Becv D, Morrison HF (1991). Borehole-to-surface electrical resistivity monitoring of salt water injection experiment. Geophy., 56: 769-777.

Bentley LR, Gharibi M (2004). Two- and three-dimensional electrical resistivity imaging at a heterogeneous site. Geophy. 69: 674-680.

Berthold S, Bentley LR, Hayashi M (2004). Integrated hydrological and geophysical study of depression-focused groundwater recharge in the Canadian prairies. Water Resour. Res., 40 W06505.

Bing Z, Greenhalgh SA (1997). A synthetic study of on cross-hole resistivity imaging with different electrode arrays. Exp. Geophy., 28: 1-5.

Bing Z, Greenhalgh SA (2000). Cross-hole resistivity tomography using different electrode configuration. Geophy. Prosp., 48: 887-912.

Binley A, Cassiani G, Middleton R, Winship P (2002). Vadose zone flow model parameterisation using cross-borehole radar and resistivity imaging. J. Hydrol., 267: 147-159.

Breier JA, Breier CF, Edmonds HN (2005). Detecting submarine groundwater discharge with synoptic surveys of sediment resistivity, radium, and salinity. Geophys. Res. Lett., 32: DOI: 10.1029/2005GL024639.

Brown D, Slater LD (1999). Focussed packer testing using geophysical tomography and CCTV in a fissured aquifer. Quart. J. Eng. Geol., 32: 173-183.

Cassiani G, Bruno V, Villa A, Fusi N, Binley AM (2006). A saline trace test monitored via time-lapse surface electrical resistivity tomography. J. Appl. Geophys., 59: 244-259

Chambers JE, Ogilvy RD, Meldrum PI, Nissen J (1999). 3D electrical resistivity imaging of buried oil-tar contaminated waste deposits. Eu. J. Environ. Eng. Geophy., 4: 3-15.

Chambers JE, Ogilvy RD, Kuras O, Cripps JC, Meldrum PI (2002). 3D electrical mapping of known targets at controlled environmental test site. Environ. Geol., 41: 690-704.

Cheng K, Simske SJ, Isaacson D, Newell JC, Gisser DG (1990). Errors due to measuring voltage on current-carrying electrodes in electric current computed tomography. IEEE Trans. Med. Imag., 37: 60-65.

Dahlin T, Loke MH (1997). Quasi-3D resistivity imaging-mapping of three-dimensional structures using two-dimensional DC resistivity techniques. Proceedings of the 3rd Meeting of the Environ. Eng. Geophy. Soc., pp. 143-146.

Christensen NB (1989). AC resistivity sounding. First Break, 7(1): 447-452.

Dahlin T, Bernstone C (1997). A roll-along technique for 3D resistivity data acquisition with multi-electrode arrays. Proceedings SAGEEP'97, Reno, Nevada, pp. 927-935.

Dahlin T, Loke MH (1997). Quasi-3D resistivity imaging-mapping of three-dimensional structures using two-dimensional DC resistivity techniques. Proceedings of the 3rd Meeting of the Environ. Eng. Geophy. Soc., pp. 143-146.

Daily W, Owen E (1991). Cross-borehole resistivity tomography. Geophy., 56: 1228-1235.

Day-Lewis FD, White EA, Johnson CD, Lane JW (2006). Continuous resistivity profiling to delineate submarine groundwater discharge – examples and limitations. The Leading Edge, 25: 724-728.

de Groot-Hedlin C, Constable SC (1990). Occam's inversion to generate smooth two- dimensional models from magnetotelluric data. Geophy., 55: 1613-1624.

Dey A, Morrison HF (1979). Resistivity modelling for arbitrarily shaped three-dimensional structure. Geophy., 44: 753-780.

Dhu T, Heinson G (2004) Numerical and laboratory investigations of electrical resistance tomography for environmental monitoring. Expl. Geophy., 35: 33-40.

Furman A, Ferre TPA, Heath GL (2007). Spatial focusing of electrical resistivity surveys considering geologic and hydrologic layering. Geophy., 72: 65-73.

Grant FS, West GF (1965). Interpretation Theory in Applied Geophysics. McGraw-Hill, New York.

Griffiths DH, Barker RD (1993). Two dimensional resistivity imaging and modelling in areas of complex geology. J. Appl. Geophy., 29: 211-226.

Griffiths DH, Turnbull J (1985). A multi-electrode array for resistivity surveying. First Break, 3: 16-20.

Griffiths DH, Turnbull J, Olayinka AI (1990). Two-dimensional resistivity mapping with a complex controlled array. First Break, 8: 121-29.

Hennig T, Weller A, Moller M (2008). Object oriented focussing of geoelectrical multielectrode measurements. J. Appl. Geophy., 65: 57-64.

Kunetz G (1966). Principles of Direct Current Resistivity Prospecting. Gebruder Borntraeger, Berlin, p. 103.

Kwon H, Kim J, Ahn H, Yoon J, Kim K, Jung C, Lee S, Uchida T (2005). Delineation of fault zone beneath a river bed by an electrical resistivity survey using a floating streamer cable. Expl. Geophy., 36: 50-58.

La Brecque DJ, Miletto M, Daily W, Ramirez A, Owen E (1996). The effect of noise on Occam inversion of resistivity tomography data. Geophy., 61: 538-548.

Leroux V, Dahlin T (2006). Time-lapse resistivity investigations for imaging saltwater transport in glaciofluvial deposits. Environ. Geol., 49: 347-358.

Li, Y, Oldenburg, DW (1994). Inversion of 3D DC resistivity data using an approximate inverse mapping. Geophy. J. Int., 116: 527-537.

Loke MH (1999). Time-lapse resistivity imaging inversion. Proceedings of the 5th Meeting of Environmental and Engineering Geophysical Society, European Section, Em1.

Loke MH, Barker RD, (1996). Practical techniques for 3D resistivity surveys and data inversion. Geophy. Prosp., 44: 499-524.

Mansoor N, Slater L (2007). Acquatic electrical resistivity imaging of shallow-water wetlands. Geophysics, 72 (5): F211-F221.

Maurer H, Boerner DE, Curtis A (2000). Design strategies for electromagnetic geophysical surveys. Inverse Problems, 16: 1097-1117.

Newmark RL, Daily WD, Kyle KR, Rimirez AL (1998). Monitoring DNAPL pumping using integrated geophysical techniques. J. Environ. Eng. Geophy., 3: 7-13

Noel M, Xu B (1991). Archaeological investigation by electrical resistivity tomography: A preliminary studies. Geophy. J. Int., 107: 95-102.

Ogilvy R, Meldrum P, Chambers J, (1999). Imaging of industrial waste deposits and buried quarry geometry by 3D tomography. European J. Environ. Eng. Geophy., 3: 103-113.

Olayinka AI (1999): Advantage of two-dimensional geoelectrical imaging for groundwater prospecting: case study from Ira, southwestern Nigeria. Water Res. J. Nig. Assoc. Hydrogeol., 10: 55-61.

Olayinka AI, Yaramanci U (1999). Choice of the best model in 2-D geoelectrical imaging: case study from a waste dump site. Eu. J. Environ. Eng. Geophy., 3: 221-244.

Oldenburg DW, Li Y (1999). Estimating depth of investigation in dc resistivity and IP surveys. Geophy., 64: 403-416.

Overmeeren RAV, Ritsema IL (1988). Continuous vertical electricalsounding. First break, 6: 313-324.

Panissod C, Michel D, Hesse A, Joivet A, Tabbagh J, Tabbagh A (1998). Recent developments in shallow-depth electrical and electrostatic prospecting using mobile arrays. Geophysics, 63: 1542-1550.

Park S (1998). Fluid migration in the vadose zone from 3D inversion of resistivity monitoring data. Geophy, 63: 41-51.

Park SK, Van GP (1991). Inversion of pole-pole data for 3D resistivity structure beneath arrays of electrodes. Geophy, 56: 951-960.

Pellerin L (2003). Characterization of an old diesel fuel spill: Results of a multi-receiver OhmMapper survey. 73rd Annual International Meeting, SEG, Expanded Abstracts, pp. 5008-5011.

Ramirez A, Daily W, LaBreque DJ, Roelant D (1996). Detection of leaks in underground storage tanks using electrical resistance methods. J. Environ Eng. Geophy., 1: 189-203.

Rein A, Hoffmann R, Dietrich P (2004). Influence of natural time-dependent variations of electrical conductivity on DC measurements. J. Hydrol., 285: 215-232.

Robinson ES, Coruh C (1988). Basic Exploration Geophysics, Wiley, New York, p. 562.

Sasaki Y (1989). Two-dimensional joint inversion of magnetotelluric and dipole-dipole resistivity data. Geophy, 54: 254-262.

Sasaki Y (1992). Resolution of resistivity tomography inferred from numerical simulation. Geophy. Prosp., 40: 453-464.

Slater L, Binley AM, Daily W, Johnson R (2000). Cross-hole electrical imaging of a controlled saline tracer injection. J. Appl. Geophy., 44: 85-102.

Slater L, Binley AM, Versterg R, Cassiani G, Birken R, Sandberg S (2002). A 3D ERT study of solute transport in a large experimental tank. J. Appl. Geophy., 49: 85-102.

Shima H (1992). 2-D and 3-D resistivity imaging reconstruction using cross-hole data. Geophy. 55: 682-694.

Sørensen KI (1996). Pulled array continuous electrical profiling. First Break, 14: 85-90.

Spies B, Ellis R (1995). Cross-borehole resistivity tomography of a pilot scale, in situ verification test. Geophy, 60: 886-898.

Stummer P, Maurer HR (2001). Real-time experimental design applied to high-resolution direct-current resistivity surveys. International Symposium on Optical Science and Technology, Expanded Abstracts, 143-150.

Stummer P, Maurer H, Green A (2004). Experimental design: electrical resistivity data sets that provides optimum subsurface information. Geophy, 69: 120-139.

Telford WM, Geldart LP, Sheriff RE, Keys DA (1976). Applied Geophysics. Cambridge University Press, Lodon, New York. p. 860.

Ward SH, Hohmann GW (1987). Electromagnetic theory for geophysical applications. In: Nabighian MN (Ed.), Electromagnetic methods in applied geophysics, Investigations in Geophysical Series, 1. SEG, Tulsa, Ok, pp. 131-312.

Wilkinson PB, Meldrum PI, Chambers JE, Kurus O, Ogilvy RD (2006). Improved strategies for the automatic selection of optimized sets of electrical resistivity tomography measurement configurations. Geophy. J. Int., 169: 1119-1126.

Xu B, Noel M (1993). On the completeness of data sets with multi-electrode systems for electrical resistivity survey. Geophy. Prosp., 41: 791-801.

Zhou W, Beck BF, Adams AL (2002). Selection of arrays to map sinkhole risk areas in karst terrain using electrical resistivity tomography. In: Symposium on Application of Geophysics to Engineering and Environmental Problems. Environ. Eng. Geophy. Soc. CDROM, paper 13CAV4.

Zhou B, Greenhalgh SA (2000). Cross-hole resistivity tomography using different electrode configurations. Geophy. Prosp., 47: 443-468.